AIAA Paper 2025-2270

Efficient Hypersonic Signature Analysis Through Amortized Inference

Ozgur Tumuklu

Mechanical, Aerospace and Nuclear Engineering

Stefan T. Radev

Department of Cognitive Science

Rensselaer Polytechnic Institute

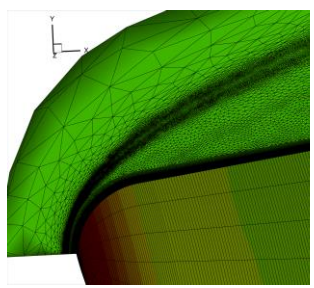

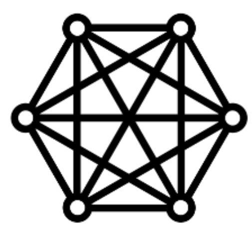

Hypersonic Aerothermal Vehicle Analysis (HAVA) Laboratory

www.havalab.org

Motivation

Complex System

High-Fidelity Simulator

Low-Fidelity Surrogates

Lower Dimensionality

Obse

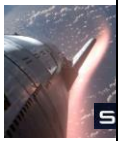

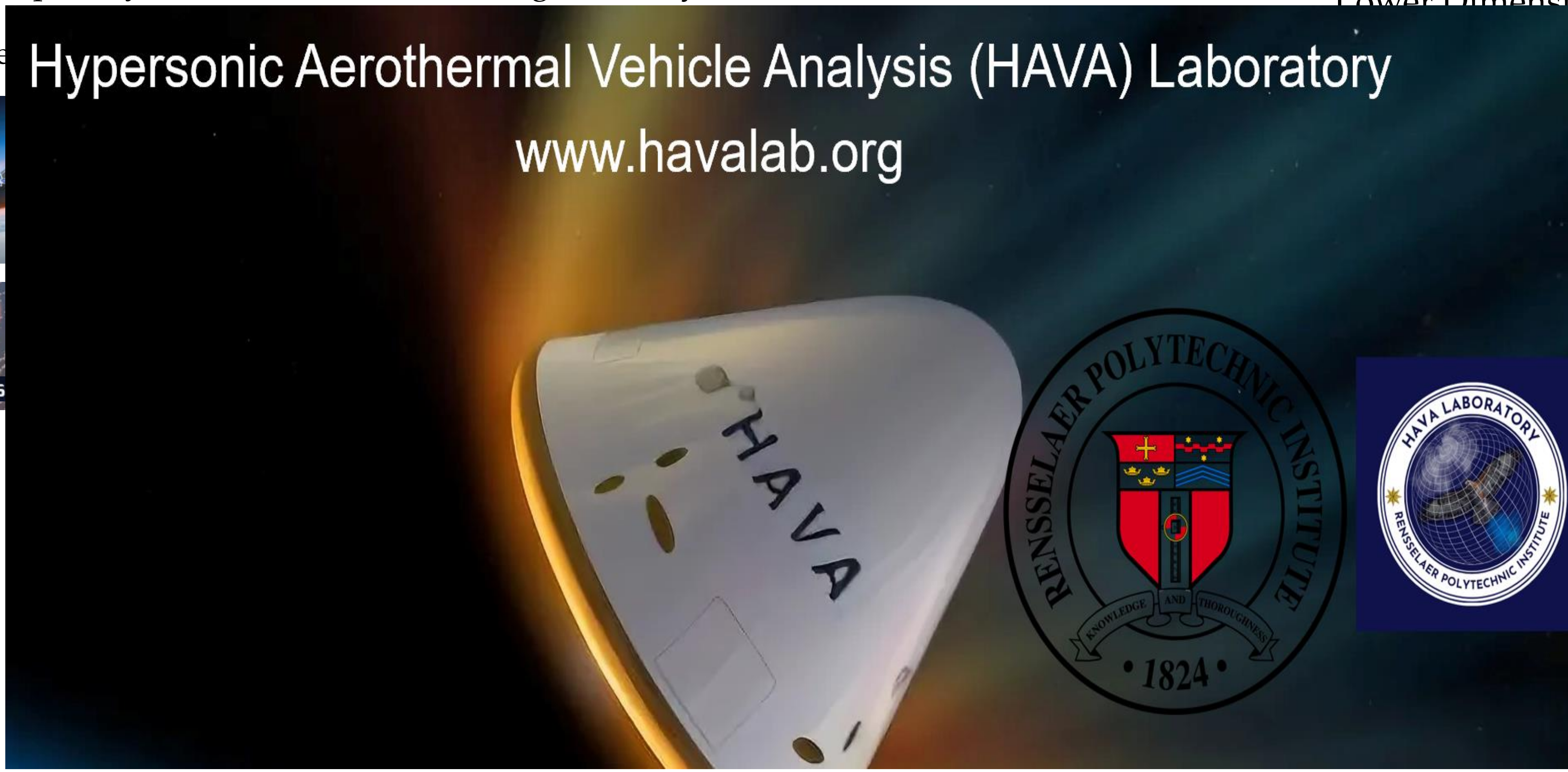

$V_d = V_{shock}$

- The **identification** and **characterization** of hypersonic radiation signatures remain challenging tasks mainly associated with **uncertainties** arising from **thermo-nonequilibrium** effects, ablation of structural elements, and turbulence.

Hypersonic Flow Solver

$$\frac{\partial \mathcal{U}}{\partial t} + \sum_{i=1}^{3} \frac{\partial(\mathcal{F}_i^c - \mathcal{F}_i^v)}{\partial x_i} = \dot{\mathcal{W}}$$

$$\mathcal{U} = \begin{Bmatrix} \rho_1 \\ \rho_2 \\ \vdots \\ \rho_s \\ \rho u_1 \\ \rho u_2 \\ \rho u_3 \\ E^{ve} \\ E \end{Bmatrix}, \quad \mathcal{F}_i^c = \begin{Bmatrix} \rho_1 u_i \\ \rho_2 u_i \\ \vdots \\ \rho_s u_i \\ \rho u_i u_1 + \delta_{i1} p \\ \rho u_i u_2 + \delta_{i2} p \\ \rho u_i u_3 + \delta_{i3} p \\ E^{ve} u_i \\ (E+p) u_i \end{Bmatrix}, \quad \mathcal{F}_i^v = \begin{Bmatrix} -\mathcal{J}_{1,i} \\ -\mathcal{J}_{2,i} \\ \vdots \\ -\mathcal{J}_{s,i} \\ -\tau_{i1} \\ -\tau_{i2} \\ -\tau_{i3} \\ -q_{ve,i} - \sum_{k=1}^{s} e_k^{ve} \mathcal{J}_{k,i} \\ -\sum_{j=1}^{3} \tau_{ij} u_j - q_{tr,i} - q_{ve,i} - \sum_{k=1}^{s} h_k \mathcal{J}_{k,i} \end{Bmatrix}$$

$$\dot{\mathcal{W}} = \begin{Bmatrix} \dot{\omega}_1 \\ \dot{\omega}_2 \\ \vdots \\ \dot{\omega}_s \\ 0 \\ 0 \\ 0 \\ \sum_{k=1}^{s} (\dot{Q}_{k,V-T} + \dot{Q}_{k,V-V} + \dot{Q}_{k,V-CH}) \\ 0 \end{Bmatrix}$$

- An open-source framework* is used to model to model.

- The solver utilizes a first-order explicit Euler scheme for time integration and employs a **second-order semi-discrete central scheme** by Kurganov*, complemented by the van Leer limiter for convective fluxes.

*Kurganov, A., and Tadmor, E., “New high-resolution central schemes for nonlinear conservation laws and convection–diffusion equations,” Journal of computational physics, Vol. 160, No. 1, 2000, pp. 241–282

OpenCFD Ltd., **OpenFOAM**: The Open Source CFD Toolbox, 2023. URL https://www.openfoam.com, retrieved from https://www.openfoam.com.

Vincent Casseau, An Open-Source CFD Solver for Planetary Entry, Ph.D. Thesis, 2017.

Numerical Schemes and Flow Conditions

Term	Schemes
Time stepping	First order Euler
Fluxes	Kurganov
Gradient	Gauss linear
Divergence	Gauss limited linear
Laplacian	Gauss linear corrected
Interpolation	vanLeer
Surface normal gradient schemes	Grad(U) corrected

Flow Parameters	Range
Pressure	[10-90] Pa
Temperature	[185-265] K
Velocity	[4500-6500] m/s

Flow Conditions for HEG-I**

Quantity	I
H_o (MJ/kg)	22.4
p_o (MPa)	35.0
T_o (K)	9200
U_∞ (m/s)	5956
p_∞ (Pa)	476
ρ_∞ (kg/m^3)	1.547×10^{-3}
T_∞ (K)	901
p_{p_∞} (kPa)	52.9
M_∞	8.98
$Y[N_2]_\infty$	0.7543
$Y[O_2]_\infty$	0.00713
$Y[NO]_\infty$	0.01026
$Y[N]_\infty$	6.5×10^{-7}
$Y[O]_\infty$	0.2283

Geuzaine, C., and Remacle, J.-F., "**Gmsh**: A 3-D finite element mesh generator with built-in pre- and post-processing facilities," , 2023. URL http://gmsh.info, version 4.9.4

**Knight, Doyle, et al. "Assessment of CFD capability for prediction of hypersonic shock interactions." *Progress in Aerospace Sciences* 48 (2012): 8-26.

Park's 11 Species Model*

Species: N_2, O_2, N, O, NO, N_2+, O_2+, N+, O+, N+, e-

Total Types of Reactions	19
Dissociation	3
Exchange	2
Associative ionization	3
Charge exchange	7
Electron impact ionization	2
Electron impact dissociation	1

O_2 + M <=> 2O + M;
N_2 + M <=> 2N + M
NO + M <=> N + O + M

*Park, C., Jaffe, R. L., & Partridge, H. (2001). Chemical-kinetic parameters of hyperbolic earth entry. *Journal of Thermophysics and Heat transfer*, *15*(1), 76-90.

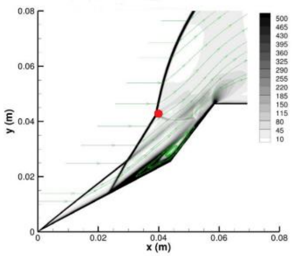

Accuracy Current Continuum Simulations over Double Wedge with Nitrogen

2D, DSMC, 98 Pa*

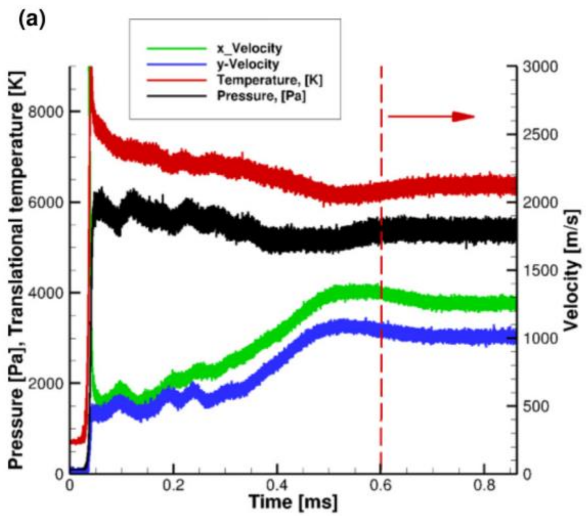

2D, NS, 98 Pa**

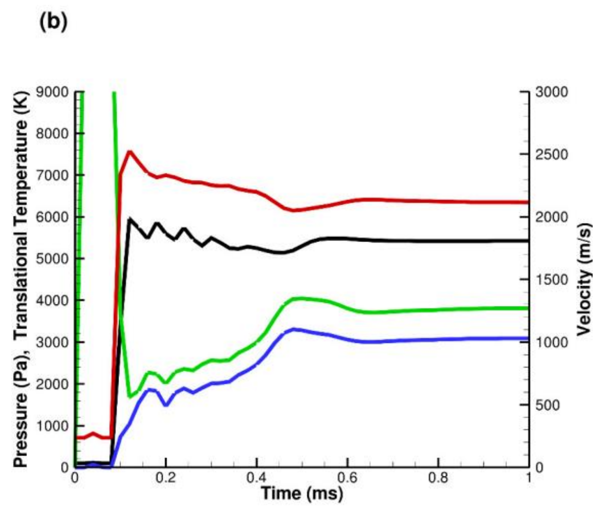

Rarefied effects**

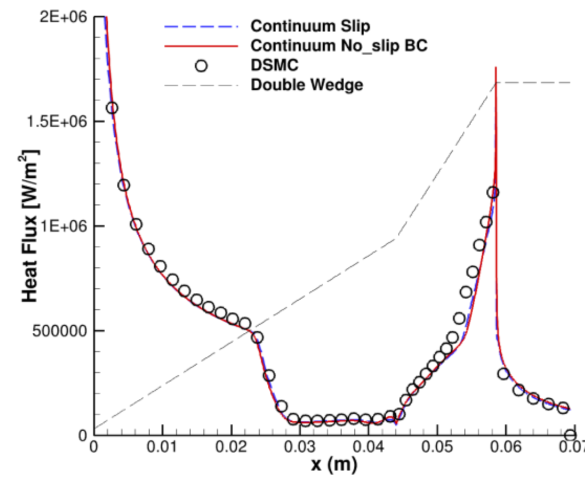

- The temporal evolutions are found to be **the same** for DSMC and NS.
- The impact of rarefied effects, even for **the lowest Re**, is negligible.

*Tumuklu, O., Levin, D. A., and Theofilis, V., “On the temporal evolution in laminar separated boundary layer shock-interaction flows using DSMC,” AIAA Paper 2017-1614, 2017.
**Tumuklu, O., and Hanquist, K. M., “Temporal characteristics of hypersonic flows over a double wedge with Reynolds number,” Physics of Fluids, Vol. 35, No. 10, 2023.

Chemistry Modeling Validation HEG-I

Park 11 Species Model

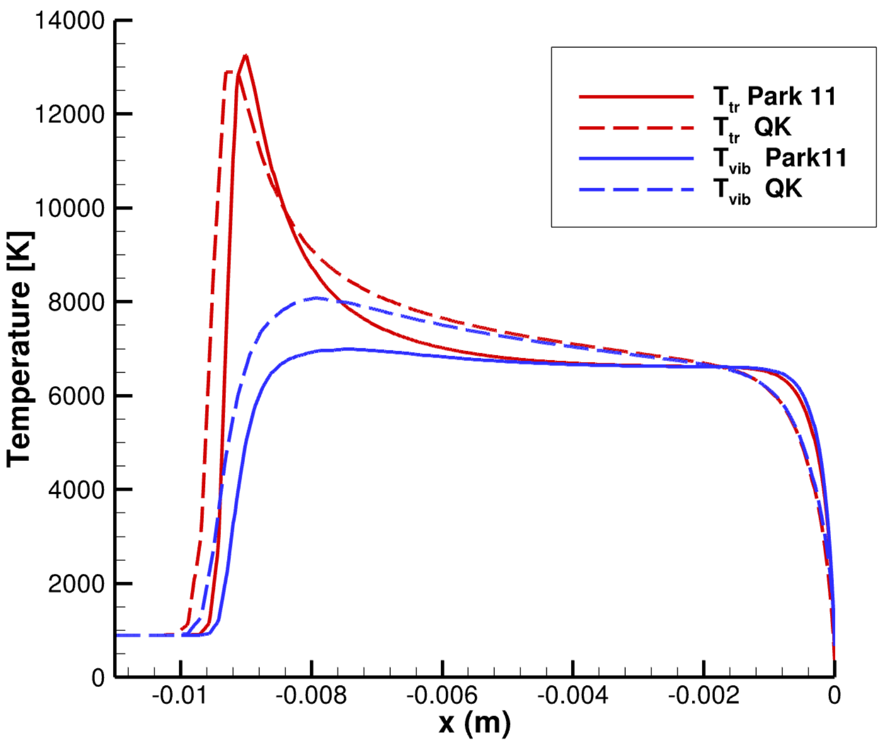

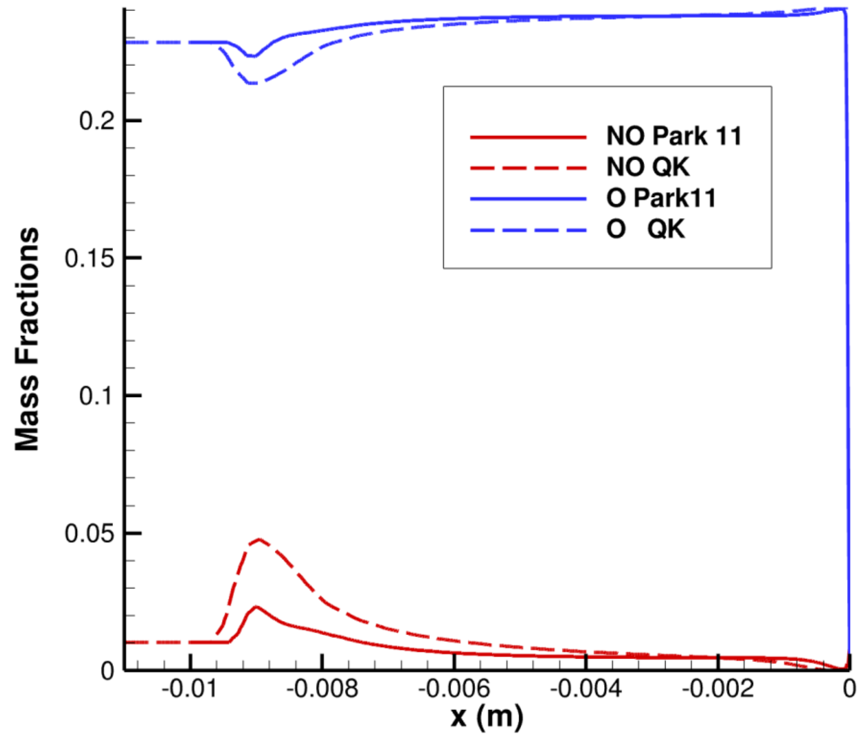

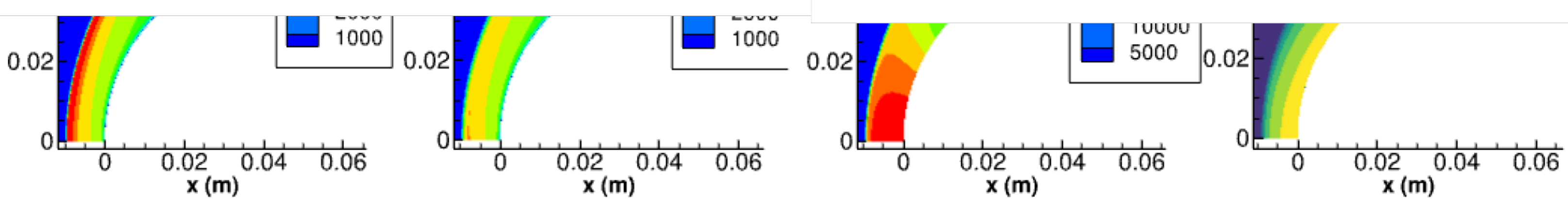

- Discrepancies are observed between two chemistry models.

Chemistry Modeling Validation HEG-1

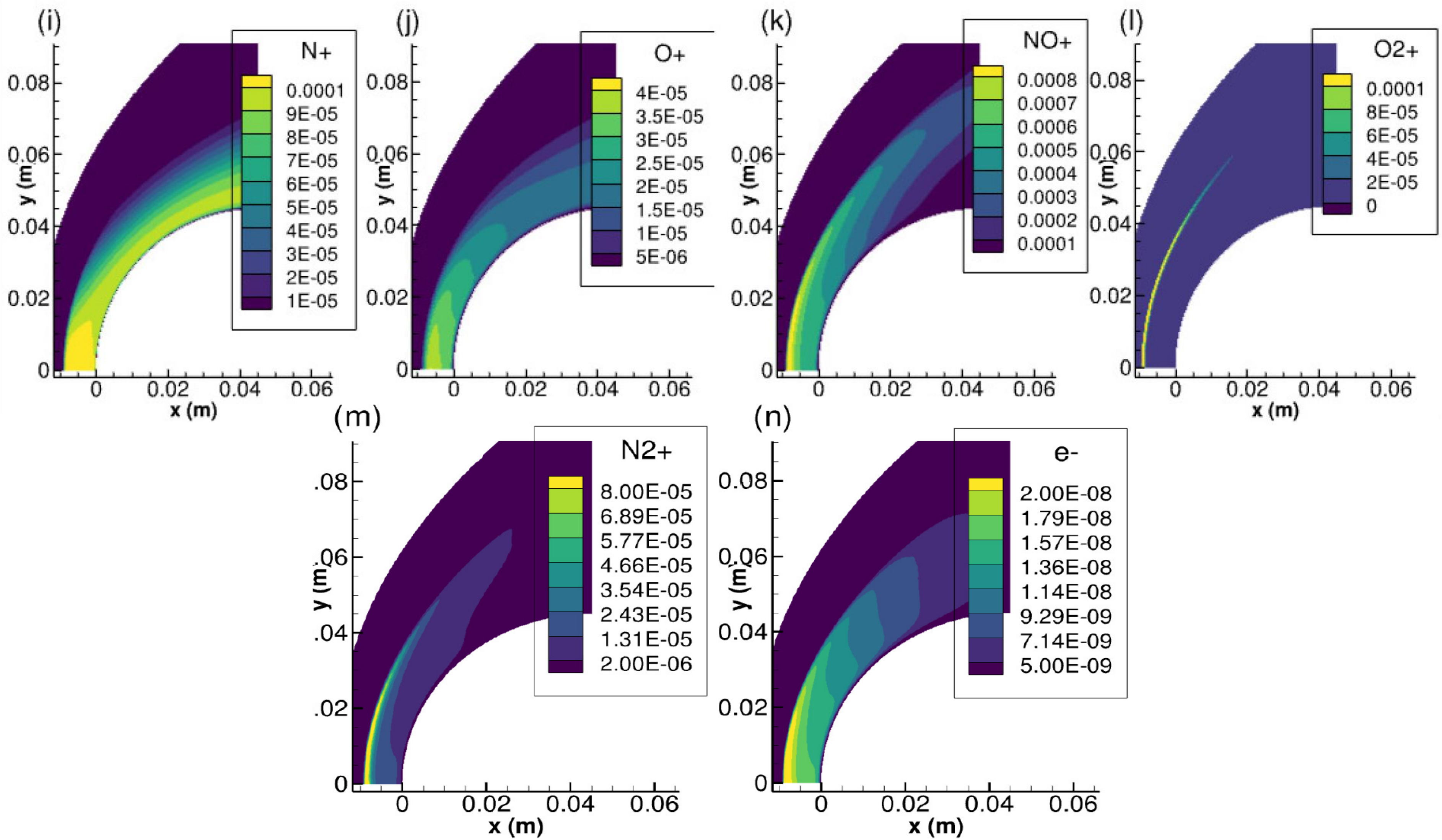

- Chemical reactions significantly modifies the flow field.
- Ionization and backward reactions are modeled.

Chemistry Modeling and Grid Convergence

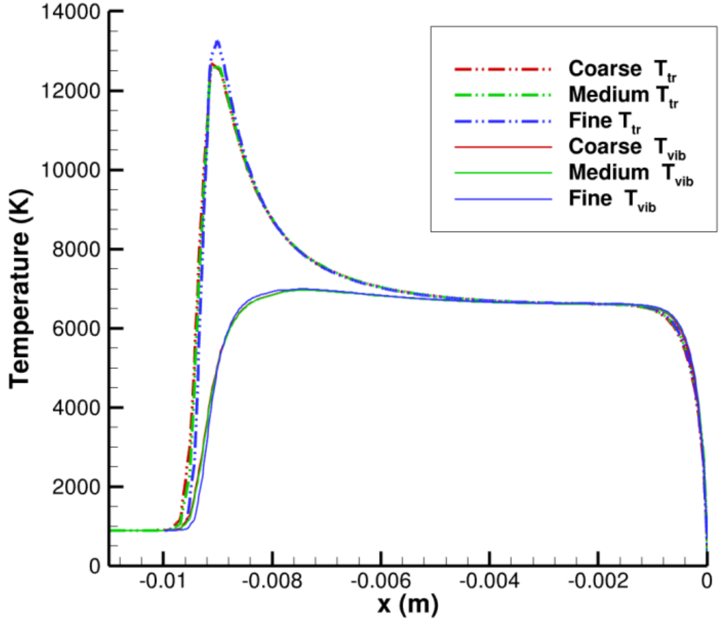

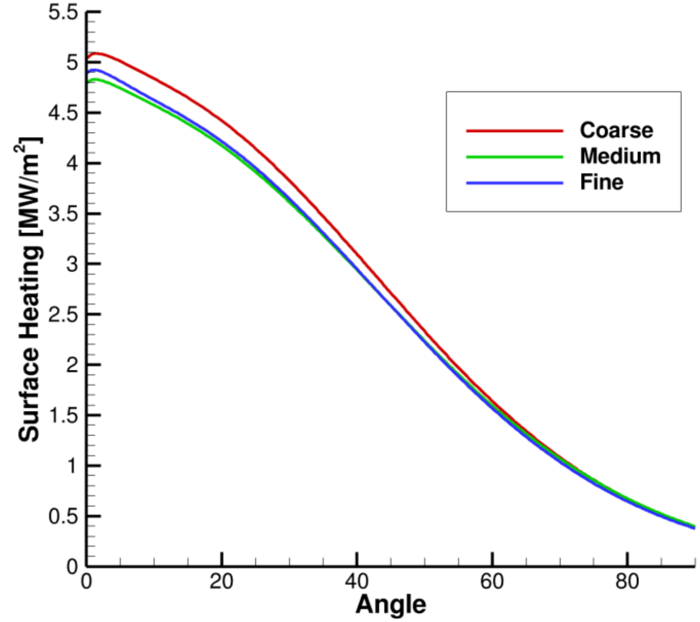

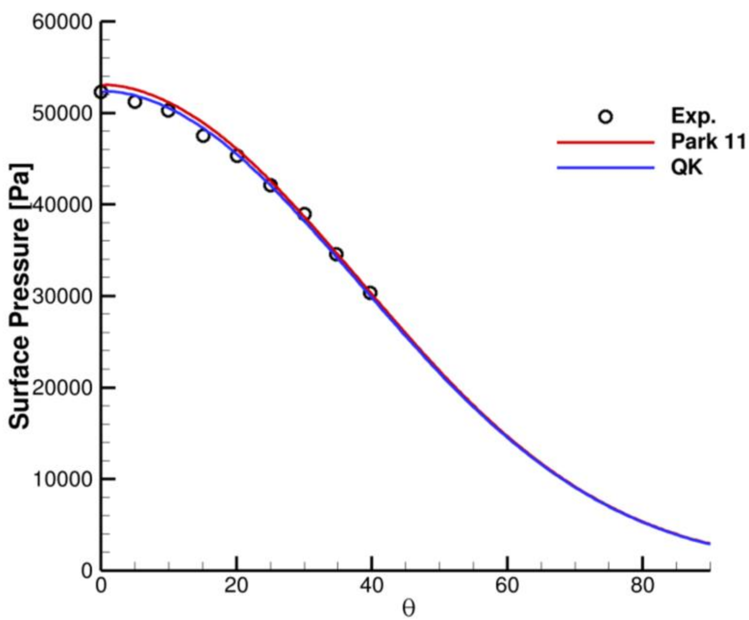

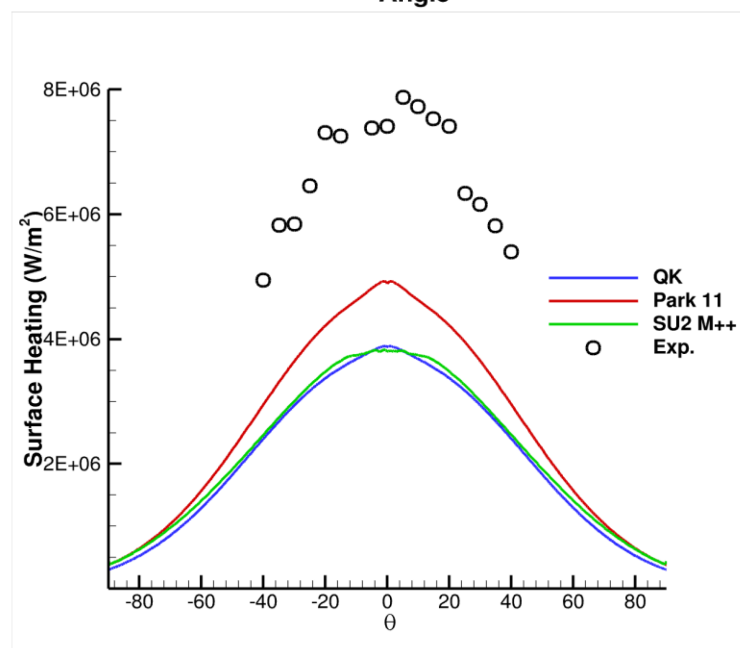

Moving Forward: Amortized Inference with BayesFlow

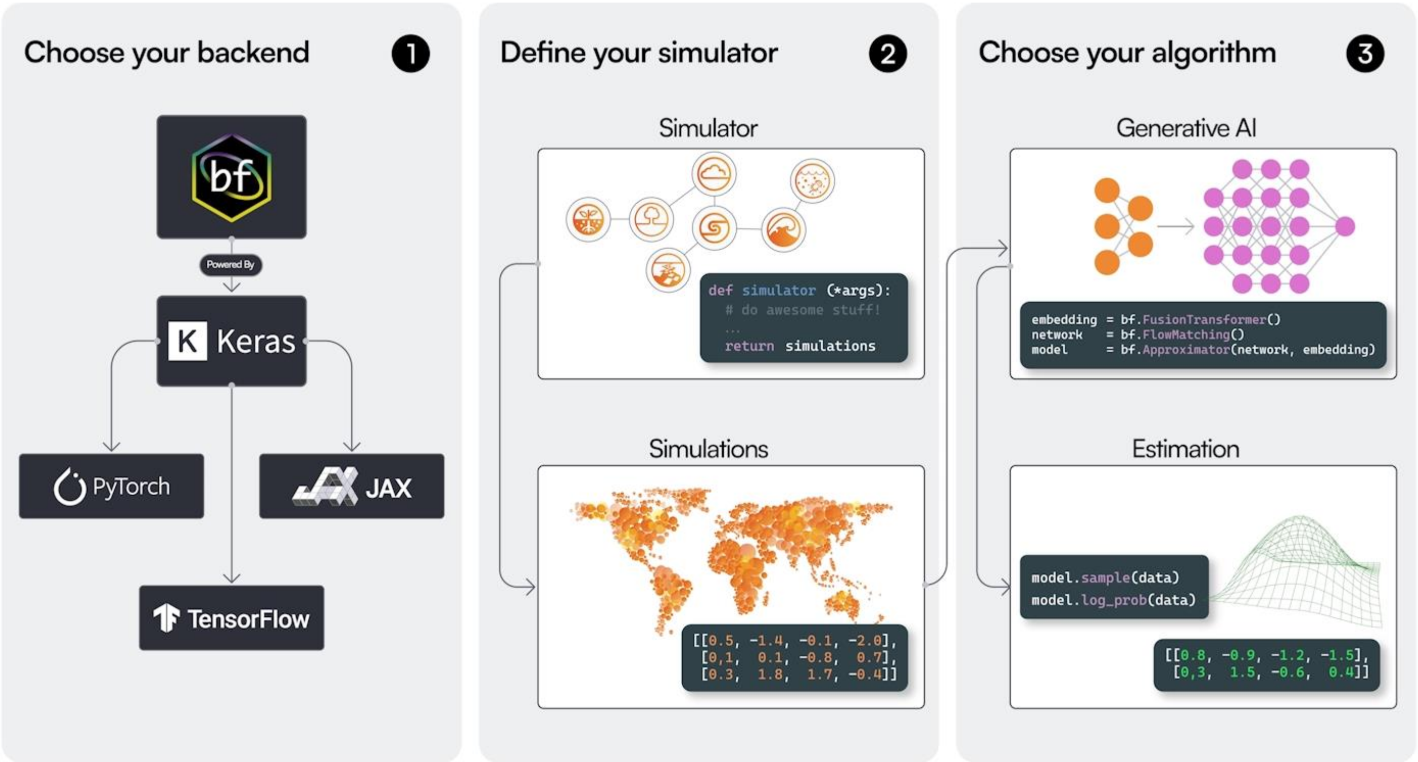

- No assumptions about **the types of data**, parameters, or distributions are made.
- A wide range of generative network architectures is used.
- The proposed approach has great potential not only for the forward problem but also for the inverse problem.
- We can approximate the **forward** or the **inverse** problem by targeting $p(\mathbf{y} \mid \boldsymbol{\theta})$ or $p(\boldsymbol{\theta} \mid \mathbf{y})$, respectively.

BayesFlow —https://bayesflow.org

Bayesian Amortized Inference

$$p(\boldsymbol{\theta} \,|\, \mathbf{y}) \propto p(\mathbf{y} \,|\, \boldsymbol{\theta})\, p(\boldsymbol{\theta}).$$

- Generative neural networks can solve challenging **inverse / forward** problems in science and engineering (Cranmer et al., 2020).

- Fully probabilistic solutions through a Bayesian lens (i.e., posterior / likelihood estimation).

- Simulation-based training of efficient (global) **neural surrogates** *q:*

$$q^* = \arg\min_{q} \mathbb{E}_{p(\boldsymbol{\theta})} \left[\mathrm{KL}(p(\mathbf{y} \,|\, \boldsymbol{\theta}) \,||\, q(\mathbf{y} \,|\, \boldsymbol{\theta})) \right]$$

- Once trained, the neural surrogate can be efficiently queried with any parameter configuration.

- For this proof of concept, we use a simpler **heteroskedastic loss** formulation**:**

$$\mathcal{L} := \mathbb{E}_{p(\boldsymbol{\theta},\mathbf{y})} \left[\sum_{i=1}^{I} \sum_{j=1}^{J} \sum_{d=1}^{D} \left(\frac{1}{2} \left(\frac{y_{ij}^{(d)} - \mu_{ij}^{(d)}(\boldsymbol{\theta}_{ij})}{\sigma_{ij}^{(d)}(\boldsymbol{\theta}_{ij})} \right)^2 + \log \sigma_{ij}^{(d)}(\boldsymbol{\theta}_{ij}) \right) \right]$$

- We report the mean (μ) and standard deviation (σ) for each surrogate distribution.

- ϴ= (Ma, Re, h_0) and $\mathbf{y} = (\mathrm{N}, \mathrm{N}_2, \mathrm{NO}, \mathrm{O}, \mathrm{O}_2)$

Dependence of Flow Field to Freestream Conditions I

Mach = 16.8, P_∞=10 Pa, and T_∞= 265 K.

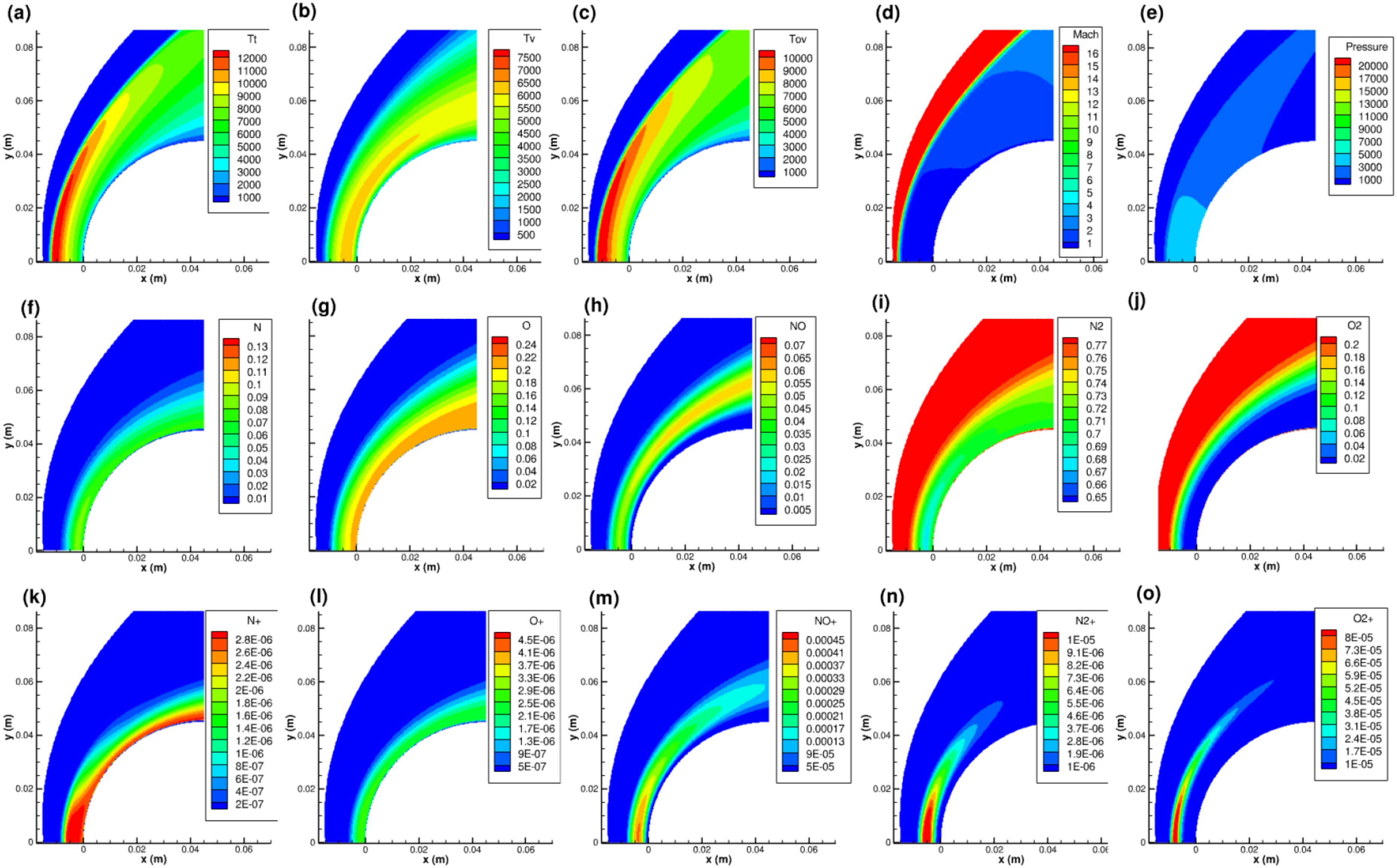

Dependence of Flow Field to Freestream Conditions II

Mach = 16.8, P_∞=90 Pa, and T_∞= 265 K.

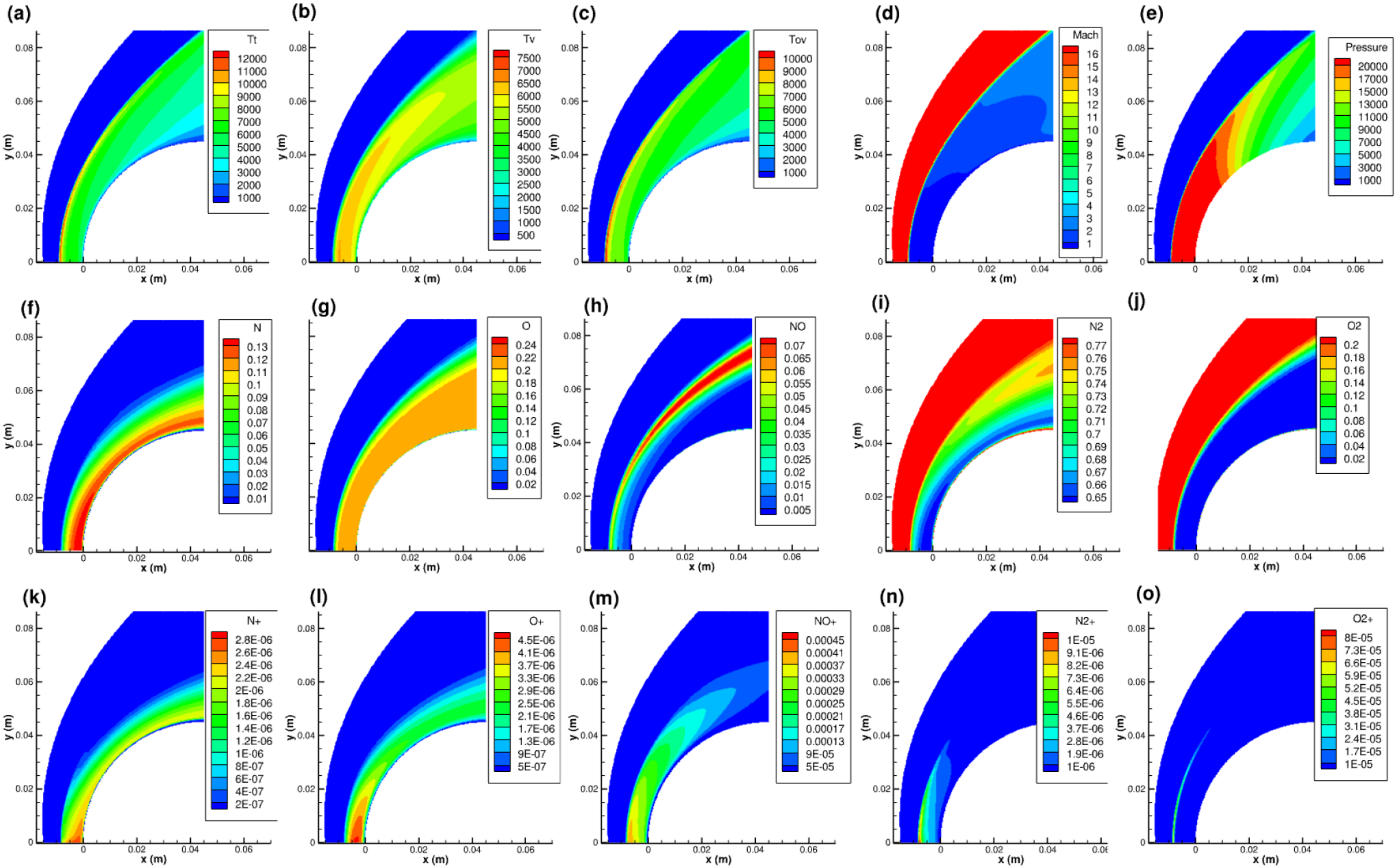

Dependence of Flow Field to Freestream Conditions III

Mach = 13.75, P_{∞}=50 Pa, and T_{∞}= 265 K.

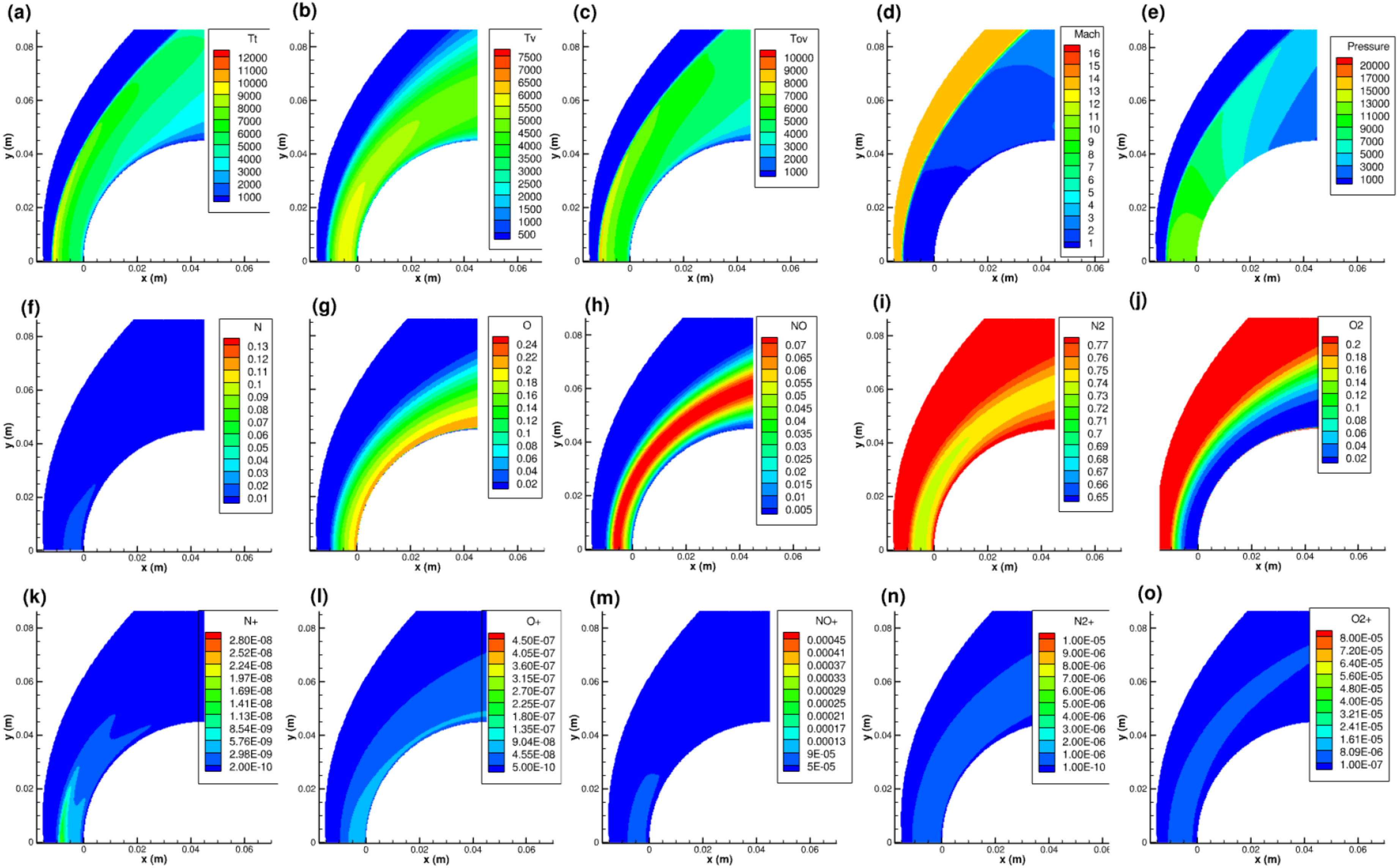

Dependence of Flow Field to Freestream Conditions IV

Mach = 19.86, P_∞=50 Pa, and T_∞= 265 K.

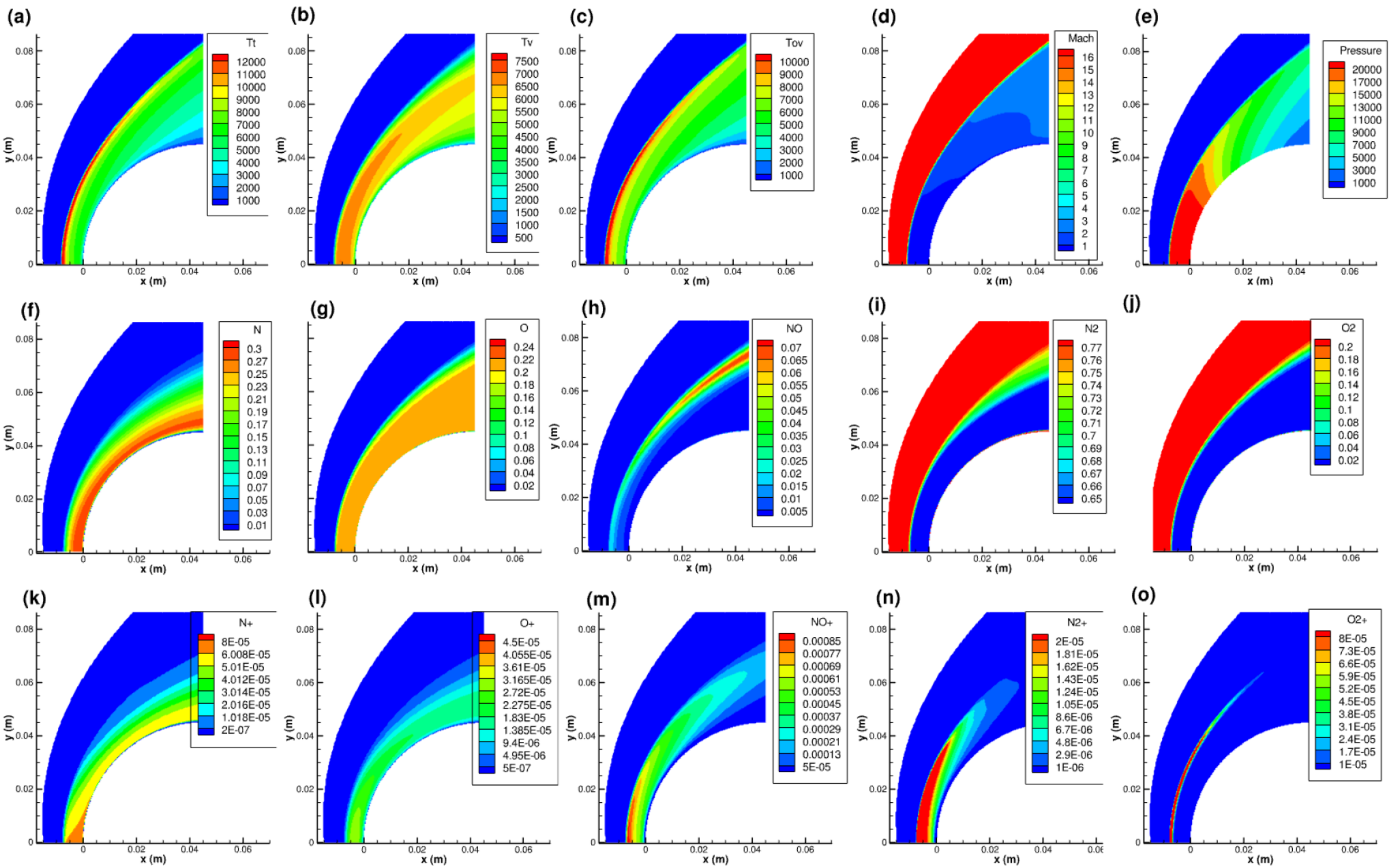

Prediction of Species Concentration I

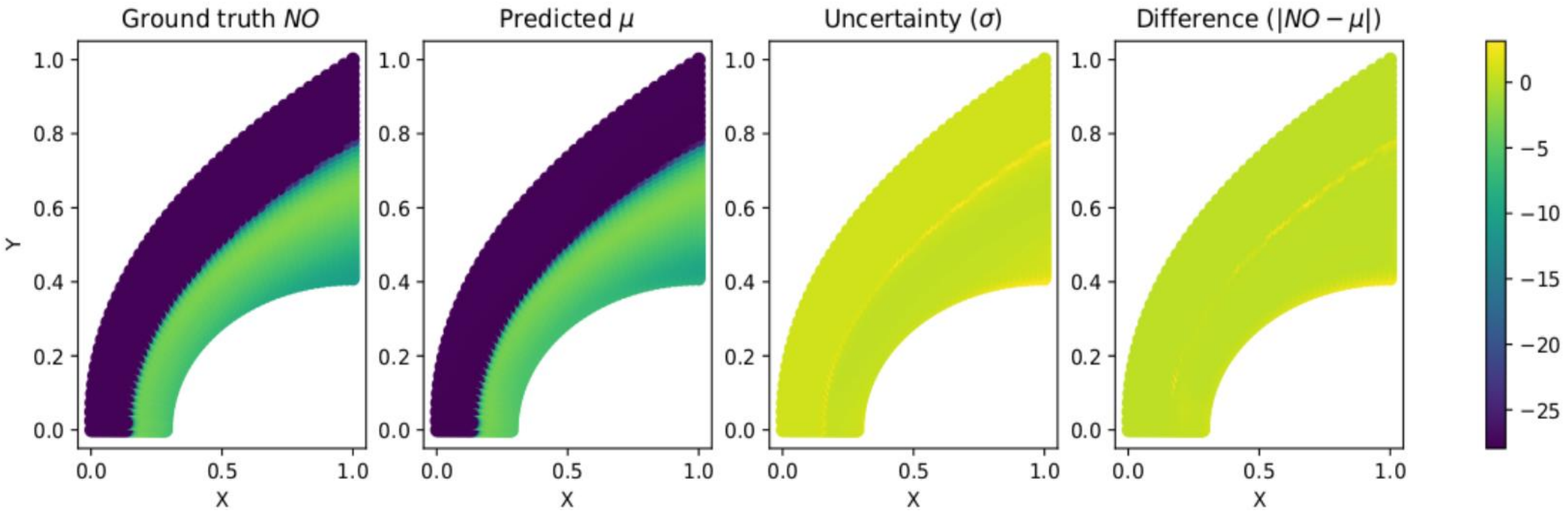

- A **logarithmic** scale is used.
- The predictions and uncertainties of log concentrations of N, O, and NO obtained on a representative low-fidelity test case simulated with a freestream axial velocity of **5481.3** m/s, a temperature of **257.75** K, and a pressure of **67** Pa are shown.
- The mean predictions (μ) closely approximate the corresponding ground-truths, while the prediction uncertainty (σ) is faithfully high for grid points where the (absolute) error is high.

Prediction of Species Concentration II

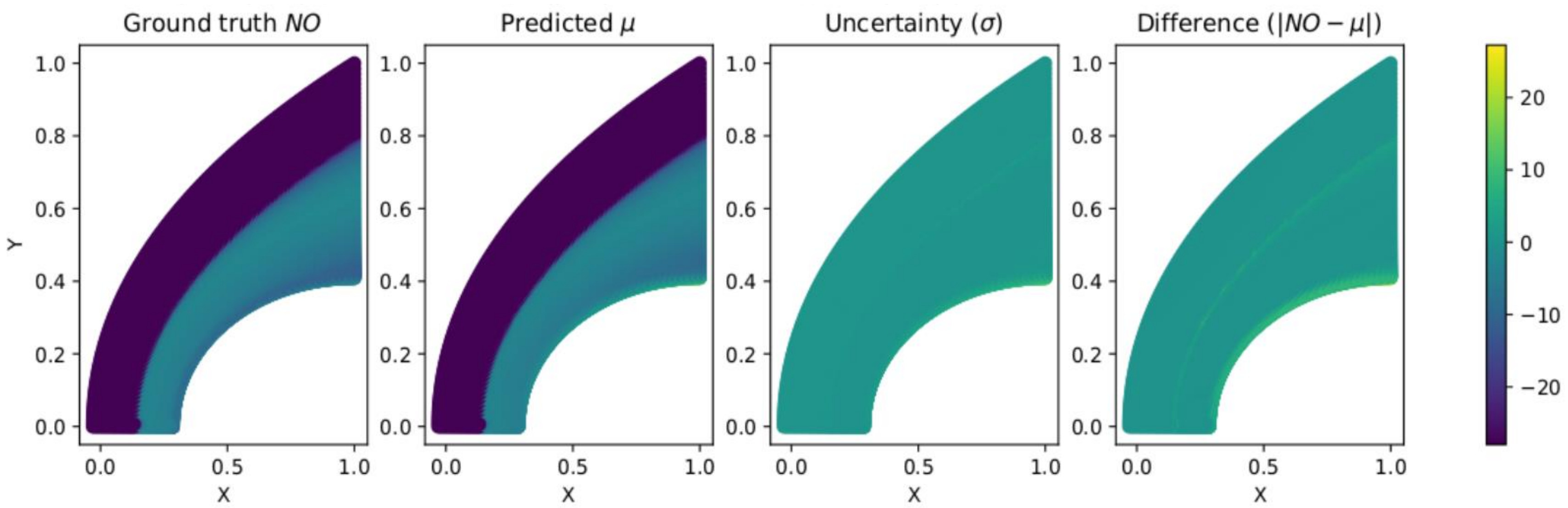

- The freestream conditions are freestream axial velocity of **5532 m/s**, a temperature of **213.4 K**, and a pressure of **41.24 Pa**.

- Even though the network is trained ***solely* on low-fidelity** simulations, it generalizes to high-fidelity cases reasonably well, while also achieving **tremendous speedups** in emulating the behavior of the simulator.

Normalized Mean Absolute Error

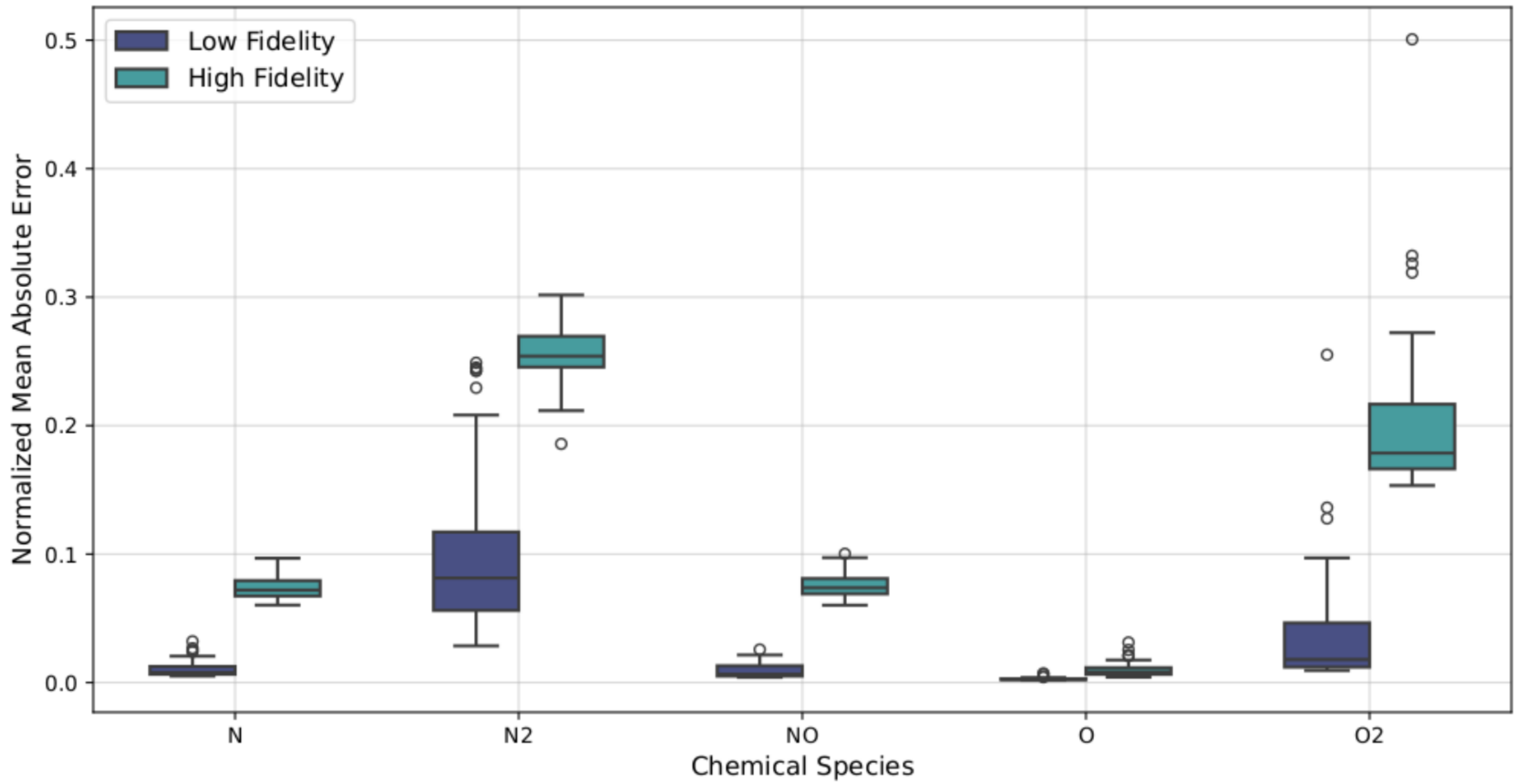

- This graph shows the network's performance on 80 low-fidelity and 80 high-fidelity test cases that **have never been seen**.
- The maximum mean error and **outliers** are observed in N_2 and O_2
- However, errors remain bounded below 0.1 NMAE for N, O, and NO, which is a highly encouraging result.

Conclusions

- The BayesFlow software was used to efficiently infer the **posterior distributions** of model parameters.

- BayesFlow can efficiently estimate the aerothermodynamic quantities of interest in hypersonic flows across different flight envelopes without **requiring time-consuming simulations**.

- Only forward problems have been demonstrated here, but we have the capability for **inverse and sensitivity** analysis.

- BayesFlow offers capabilities to generalize to unseen parameter configurations and fidelity levels, replacing traditional lookup tables in aero databases for broader-spectrum design applications.

Acknowledgements

- The computational resources are granted by NSF-ACCESS for the projects of PHY240018 PHY240112 through Purdue's Anvil cluster.
- Financial support for this research was provided by RPI.
- The authors are grateful to Batuhan Yalcin for his assistance with the scripts for running 2000 different cases.

Thank you.